Article:
Rucklidge, A.M. (2001) Global bifurcations in the Takens-Bogdanov normal form with D_4 symmetry near the O(2) limit. Physics Letters A, 284 (2-3). pp. 99-111. ISSN: 0375-9601

https://doi.org/10.1016/S0375-9601(01)00276-6

Submitted to *Physics Letters A* 24/4/2001

Global bifurcations in the Takens–Bogdanov normal form with D_4 symmetry near the $O(2)$ limit

A.M. Rucklidge [1]

Department of Applied Mathematics,
University of Leeds, Leeds, LS2 9JT, UK

Abstract

The dynamics of the normal form of the Takens–Bogdanov bifurcation with D_4 symmetry is governed by a one-dimensional map near the gluing bifurcation and near the $O(2)$ integrable limit, rather than the three-dimensional map one would expect. This great simplification allows a quantitative description of the bifurcation sequence through which stability is transfered between invariant subspaces.

Key words: 05.45+b 47.20.Ky 47.52.+j 47.54.+r 47.65+a
Gluing bifurcation, symmetry, chaos, magnetoconvection.

1 Introduction

The Takens–Bogdanov bifurcation arises in many physical problems, notably in convection where the destabilizing temperature gradient competes with a stabilizing salt gradient, Coriolis force, magnetic field or other effect [1–6]. To be definite, consider the stabilizing effect to be an imposed vertical magnetic field: if the field is weak, the initial instability from a state of no motion to convection is a steady bifurcation (pitchfork); with stronger fields and low magnetic diffusivity, the primary bifurcation is oscillatory (Hopf) [1]. In constrained geometries, there is a codimension-two Takens–Bogdanov bifurcation, at which the pitchfork and Hopf bifurcations coincide.

The symmetry of the container in which convection takes place plays a key role in determining the dynamics near the Takens–Bogdanov bifurcation. With the assumption of a three-dimensional flow confined to an $L \times L \times 1$ box with

[1] E-mail: A.M.Rucklidge@leeds.ac.uk

square cross-section, reflections and 90° rotation symmetries (which generate the group D_4) of the container lead to a fourth-order normal form near the Takens–Bogdanov bifurcation:

$$\ddot{u} = -\lambda u + \kappa \dot{u} + Pu^3 + Qu^2\dot{u} + Rv^2u + Sv\dot{v}u + Tv^2\dot{u} + Uv\dot{v}\dot{u}, \tag{1}$$

$$\ddot{v} = -\lambda v + \kappa \dot{v} + Pv^3 + Qv^2\dot{v} + Ru^2v + Su\dot{u}v + Tu^2\dot{v} + Uu\dot{u}\dot{v}, \tag{2}$$

where u and v represent the amplitude of the two marginally stable modes of convection, $P, \ldots, U$ are constants, the dot stands for differentiation with respect to time, and κ and λ are unfolding parameters that are zero at the codimension-two bifurcation point [7]. In a typical example, u and v would be the amplitudes of orthogonal convection rolls with their axes oriented in two horizontal directions. The two reflections $\mathcal{R}_1$ and $\mathcal{R}_2$ that generate the group D_4 act on the mode amplitudes as

$$\mathcal{R}_1 : (u, v) \to (-u, v), \qquad \mathcal{R}_2 : (u, v) \to (v, u). \tag{3}$$

Note that the form of the ordinary differential equations (ODEs) (1–2) differs from that in [7] owing to a different choice of normal form transformations, but the two are equivalent.

These equations have been known for many years, but progress with their analysis has been limited. Early numerical work [7] revealed regions in parameter space in which the equations have chaotic trajectories, as has more recent work on the hexagonal version of this problem [8]. A natural supposition is that these chaotic trajectories are associated with global bifurcations of one type or another. However, a detailed analysis of the dynamics near these global bifurcations has so far not been carried out (though Matthies [9] has recently made progress on the symbolic dynamics of trajectories near homoclinic bifurcations in the D_3 case).

In order to understand why progress has been held back, it is necessary to turn briefly to the second-order normal form obtained by restricting to the invariant subspace $v = 0$:

$$\ddot{u} = -\lambda u + \kappa \dot{u} + Pu^3 + Qu^2\dot{u}. \tag{4}$$

(The subspace $u = 0$ is equivalent, and a similar equation is found in the invariant subspaces $u = \pm v$.) The behaviour of this equation is well understood [2,10]. The primary pitchfork bifurcation occurs when $\lambda = 0$ and the primary Hopf bifurcation requires $\kappa = 0$ and $\lambda > 0$, and there are a variety of secondary local and global bifurcations. To be specific, take P to be negative and Q positive, so the pitchfork is supercritical and the Hopf is subcritical. In this case, the behaviour of the system for (κ, λ) close to zero is depicted in figure 1(a): representative phase portraits are shown between the lines of pitchfork (pf), Hopf, saddle-node and global (gluing) bifurcations. Bifurcations sequences along two cuts across this diagram are shown in figure 1(b,c).

At the gluing bifurcation, two stable periodic orbits created in the Hopf bifurcation from the two nontrivial equilibria collide at the origin in a global bifurcation, and glue together to form a larger periodic orbit that encircles all three equilibria.

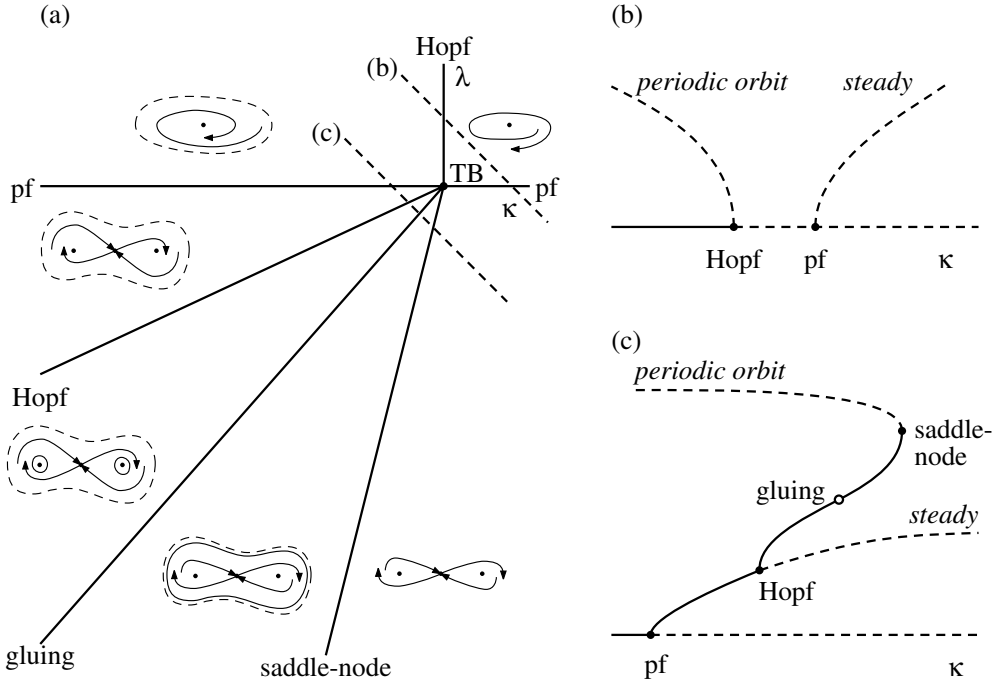

Fig. 1. Behaviour of (4) with $P < 0$ and $Q > 0$ [10]. (a) Unfolding diagram, with phase portraits in the $(u, \dot{u})$ plane inset. (b,c) Bifurcation diagrams along two one-dimensional sections (dashed lines in (a)) through the (κ, λ) plane, taken on either side of the Takens–Bogdanov (TB) point. Stable steady solutions and periodic orbits are shown with solid lines; unstable solutions are shown as dashed lines. In (b,c), local bifurcations are shown as filled circles and global bifurcations as open circles.

The presence of the gluing bifurcation can be established by considering the limit of small (κ, λ) [10]. Scaling (κ, λ) by ϵ^2 ($\epsilon \ll 1$) forces the parameters to be close to the Takens–Bogdanov point, and an appropriate balance of terms in the ODEs is obtained by scaling u by ϵ and time by $1/\epsilon$. In this limit, the first derivative terms, involving $\dot{u}$, go to higher order than the other terms when $\epsilon \to 0$, and one obtains ODEs that are Hamiltonian and integrable:

$$H(u, \dot{u}) = \frac{1}{2}\dot{u}^2 + \frac{\lambda}{2}u^2 - \frac{P}{4}u^4, \qquad \text{with} \qquad \dot{H} = \epsilon(\kappa + Qu^2)\dot{u}^2. \tag{5}$$

The ODE $H =$ constant results in trajectories that are all closed loops, with $H = 0$ corresponding to orbits involved in the gluing bifurcation. The leading order condition for the gluing bifurcation is that $\int \dot{H}\, \mathrm{d}t = 0$ around one of

these orbits. This can readily be shown to lead to

$$\kappa = -\frac{4}{5}\frac{Q}{P}\lambda + \mathcal{O}(\epsilon) \qquad \text{with } \lambda < 0. \tag{6}$$

Within the $u = v$ invariant subspace, the gluing bifurcation occurs at a similar value of κ, but with P replaced by $P + R$ and Q replaced by $Q + S + T$ in the expression above.

In the fully three-dimensional case, the same Hamiltonian limit yields

$$H(u, \dot{u}, v, \dot{v}) = \frac{1}{2}(\dot{u}^2 + \dot{v}^2) + \frac{\lambda}{2}(u^2 + v^2) - \frac{P}{4}(u^4 + v^4) - \frac{1}{2}Ru^2v^2, \tag{7}$$

with $\dot{H} = \mathcal{O}(\epsilon)$. The difficulty here is that even in the limit $\epsilon \to 0$, the system is not completely integrable, so trajectories on the surface $H =$ constant need not be closed. In particular, trajectories that approach one of the equilibrium points will typically be chaotic (see figure 2), so there is no simple criterion for the existence of global bifurcations.

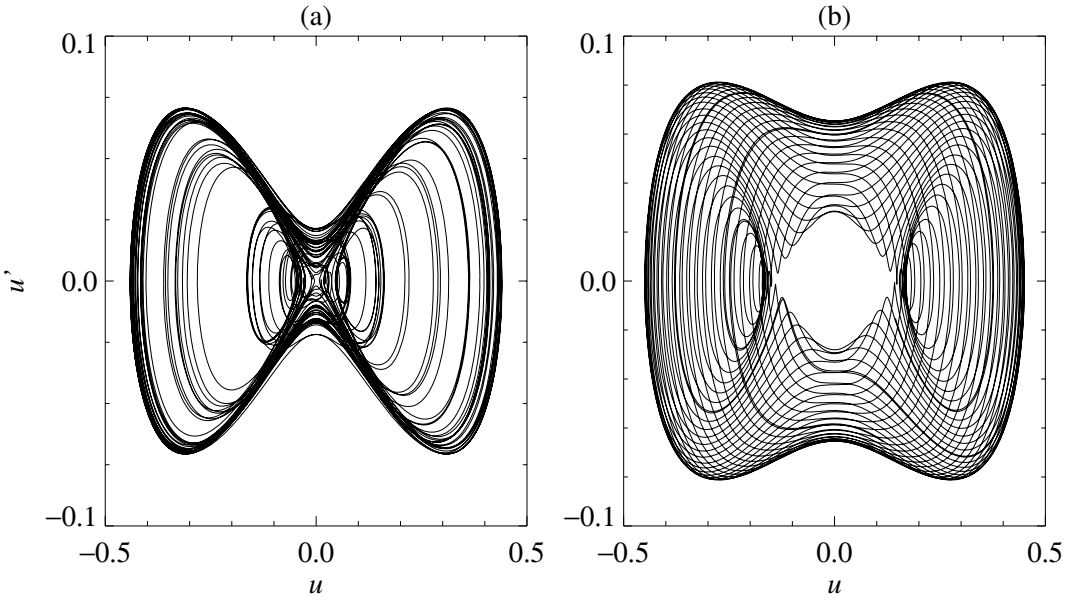

Fig. 2. Phase portraits of (1–2) in the Hamiltonian limit, starting from two initial conditions. Parameter values were: $\lambda = -0.1$, $\kappa = Q = S = T = U = 0$, $P = -1.0378$ and $R = -1.0686$ (derived from $L^2 = 0.01$ in (8–10)). (a) Chaotic trajectory started near the origin; (b) quasi-periodic trajectory.

There are at least three cases in which a second integral can be found, rendering the Hamiltonian limit integrable [7,11]. In two of these cases ($R = 0$ and $R = 3P$), the fourth-order ODEs decouple into two sets of second order ODEs with separate Hamiltonian functions; in the third case ($P = R$), the Hamiltonian limit becomes $O(2)$ (circularly) symmetric with a second integral $u\dot{v} - v\dot{u}$ [12]. The $O(2)$ limit is interesting because near the gluing bifurcation,

trajectories leaving a neighbourhood of the origin will all return to the origin regardless of the direction in which they left – this is not true in general. It is this observation that allows progress to be made.

This paper focuses on gluing bifurcations near the D_4-symmetric Takens–Bogdanov bifurcation in the nearly-$O(2)$ limit, taking as an example a model of three-dimensional convection with an imposed vertical magnetic field. Near the global bifurcation, maps are constructed that describe the dynamics of trajectories that pass close to the origin, rather than by averaging over trajectories. A three-dimensional map would normally be needed to describe the dynamics of a fourth-order set of ODEs, but near the $O(2)$ limit, the map (surprisingly) reduces to one dimension.

This work is relevant not only to three-dimensional magnetoconvection in narrow containers, but also to two main classes of other problems. Over the years there has been a great deal of interest in Takens–Bogdanov bifurcations in two-dimensional pattern-forming problems with $O(2)$ symmetry arising from periodic side boundary conditions, cumulating in the work of Dangelmayr & Knobloch [12]. More recently, it has been realised that breaking a symmetry can lead to complex dynamics in a system that originally behaved in a simple fashion: see for example [13–15], where weak symmetry breaking arises as a result of distant side walls and can lead to bursting dynamics, and [16] where $O(2)$ symmetry is brought down to D_4 by externally imposed corrugations on the lower boundary. In these problems, it is appropriate to consider weak symmetry-breaking effects: in the example under investigation here, simple behaviour (a gluing bifurcation of periodic orbits) becomes much more complicated and interesting once the perfect $O(2)$ symmetry is weakly broken.

The second main area of relevance is to problems posed in square containers, or secondary instabilities of patterns with square symmetry, as in [17,18], for example. The D_4 symmetry of these problems cannot be treated as weakly broken $O(2)$, but the hope is that the structure that appears in the $O(2)$ limit acts as an organising centre for the dynamics observed away from this limit.

The magnetoconvection model is presented in section 2, and the derivation of the one-dimensional map (by first constructing a three-dimensional map) is in section 3. Bifurcations in the map and in the normal form are analysed in section 4. Finally, the significance of these results is discussed in section 5.

2 Magnetoconvection in a narrow container

The PDEs describing three-dimensional incompressible convection in the presence of a vertical magnetic field are well known [4], and the procedure for computing the coefficients in the normal form (1–2) at the Takens–Bogdanov point is standard if time-consuming [2,3]. Since this paper is concerned with the behaviour of the normal form rather than behaviour of a specific convection problem, illustrative parameter values are taken: the Prandtl number

$\sigma = 1$ and the magnetic diffusivity ratio $\zeta = 0.8$. The linear unfolding parameters κ and λ will then depend on the strength of the magnetic field and the temperature difference across the layer, but are zero at the Takens–Bogdanov point [3]. The cubic coefficients P, ..., U can be computed at the Takens–Bogdanov point and depend only on the size L of the container. General values of the physical properties result in a normal form without any special features, but explicit computation of the normal form coefficients reveals that in the limit $L \to 0$ (i.e., magnetoconvection in a narrow container), the normal form gains $O(2)$ (circular) symmetry. With $L \ll 1$, the normal form coefficients are

$$P = -1 - \frac{34}{9}L^2 + \mathcal{O}(L^4), \qquad R = -1 - \frac{1667}{243}L^2 + \mathcal{O}(L^4), \tag{8}$$

$$Q = 2 - \frac{33}{7}L^2 + \mathcal{O}(L^4), \qquad S = 2 - \frac{8}{7}L^2 + \mathcal{O}(L^4), \tag{9}$$

$$T = -\frac{25}{7}L^2 + \mathcal{O}(L^4), \qquad U = \frac{50}{7}L^2 + \mathcal{O}(L^4). \tag{10}$$

These expressions can also be obtained by taking the limit of a narrow container before going to the Takens–Bogdanov point, as in [19,20].

When $L = 0$, the D_4-symmetric normal form (1–2) acquires $O(2)$ symmetry, where the rotations in $O(2)$ act as standard rotations in the (u, v) plane. The $O(2)$ symmetry requires $P = R$, $Q = S + T$ and $U = 0$, although the $O(2)$-symmetric normal form would usually have an additional term not found in (1–2). The aspect ratio L is used to control the degree to which the $O(2)$ symmetry is broken.

3 Derivation of the one-dimensional map

Gluing bifurcations occur in both the $v = 0$ and the $u = v$ invariant subspaces (as well as the conjugate $u = 0$ and $u = -v$ subspaces) at $\kappa = (\frac{8}{5} - \frac{83484}{8505}L^2)\lambda + \mathcal{O}(L^4, \lambda^2)$ and at $\kappa = (\frac{8}{5} - \frac{104456}{8505}L^2)\lambda + \mathcal{O}(L^4, \lambda^2)$. In general, these bifurcations occur at different parameter values, but in the $O(2)$ limit ($L = 0$), the parameter values of the two gluing bifurcations coincide. This is a consequence of the rotational symmetry: the behaviour of a trajectory does not depend on the direction in which it leaves the origin, and close to the gluing bifurcation, all trajectories that leave along $\mathcal{W}^{\mathrm{u}}$, the unstable manifold of the origin, will return to a neighbourhood of the origin. Close to the $O(2)$ limit ($L \ll 1$), the coincidence of the gluing bifurcations in the $v = 0$ and $u = v$ invariant subspaces is only weakly broken. Therefore, near the gluing bifurcations, trajectories that start near the origin will leave along the two-dimensional unstable manifold $\mathcal{W}^{\mathrm{u}}$ and return to a neighbourhood of the origin even if they are not close to one of the invariant subspaces.

In the following derivation, attention is confined to trajectories that repeatedly come within a certain distance $h \ll 1$ from the origin. For a fixed value of h,

there will be a range of parameter values close to the gluing bifurcation and a range of values of $L^2 \ll 1$ in which all trajectories leaving the origin close enough to the unstable manifold will return to within h of the origin. Thus the accuracy of the approximations made below is improved by making h smaller, and by implication choosing parameters closer to the gluing bifurcation and smaller values of L^2.

The construction of a map that describes the dynamics of these trajectories follows standard methods [10]. It is convenient to change coordinates before constructing the map. The linearised dynamics near the origin has eigenvalues $\lambda_\pm = \frac{1}{2}(\kappa \pm \sqrt{\kappa^2 - 4\lambda})$, each of multiplicity two. The eigenvectors form a basis for a coordinate system, changing from $(u, \dot{u})$ to (x, α) and $(v, \dot{v})$ to (y, β), where (x, y) are in the stable direction and (α, β) are in the unstable direction. In addition, two polar coordinate systems are useful, with (r, θ) in the (x, y) plane and (ρ, ϕ) in the (α, β) plane. In these coordinates, the linearised equations near the origin take the form:

$$\dot{x} = \lambda_- x, \qquad \dot{y} = \lambda_- y, \qquad \dot{r} = \lambda_- r, \qquad \dot{\theta} = 0, \tag{11}$$

$$\dot{\alpha} = \lambda_+ \alpha, \qquad \dot{\beta} = \lambda_+ \beta, \qquad \dot{\rho} = \lambda_+ \rho, \qquad \dot{\phi} = 0. \tag{12}$$

Freely switching between coordinate systems keeps the size of later expressions to a minimum.

The return map will be from a three-dimensional Poincaré section at $r = h \ll 1$ to itself, but an intermediate section at $\rho = h$ is also needed. Close to the origin, points on $r = h$ are mapped to $\rho = h$ according to:

$$(h, \theta, \rho, \phi) \to (r_1, \theta_1, h, \phi_1) = \left(h \left(\frac{\rho}{h} \right)^\delta, \theta, h, \phi \right), \tag{13}$$

where $\delta = -\lambda_-/\lambda_+$. This map is $O(2)$-symmetric since the terms in (1–2) that break that symmetry are all nonlinear. The second part of the map, from $\rho = h$ back to $r' = h$, must respect the D_4 symmetry and so takes the form:

$$x' = x_1 f_1(x_1^2, y_1^2, \alpha_1^2, \beta_1^2, L^2) + \alpha_1 f_2(x_1^2, y_1^2, \alpha_1^2, \beta_1^2, L^2) \tag{14}$$

$$\alpha' = x_1 f_3(x_1^2, y_1^2, \alpha_1^2, \beta_1^2, L^2) + \alpha_1 f_4(x_1^2, y_1^2, \alpha_1^2, \beta_1^2, L^2) \tag{15}$$

$$y' = y_1 f_1(y_1^2, x_1^2, \beta_1^2, \alpha_1^2, L^2) + \beta_1 f_2(y_1^2, x_1^2, \beta_1^2, \alpha_1^2, L^2) \tag{16}$$

$$\beta' = y_1 f_3(y_1^2, x_1^2, \beta_1^2, \alpha_1^2, L^2) + \beta_1 f_4(y_1^2, x_1^2, \beta_1^2, \alpha_1^2, L^2) \tag{17}$$

with $x'^2 + y'^2 = r'^2 = h^2$, and $f_1, \ldots, f_4$ smooth functions. While (14–17) has the appearance of being a four-dimensional map, in fact the constraint $r' = h$ reduces the dimension to three: this can be brought out by writing $\theta' = \tan^{-1}(y'/x')$ and $r' = h$ instead of equations for x' and y'.

The usual approach at this stage is to expand the functions $f_1, \ldots, f_4$ as Taylor series in their arguments, which are small for trajectories close to $\mathcal{W}^{\mathrm{u}}$, for parameters close to the gluing bifurcation and close to the $O(2)$ limit.

Before doing this, we first recover the map that describes the standard gluing bifurcation in the $O(2)$ symmetric case, with $L^2 = 0$.

Approximating the four functions $f_1, \ldots, f_4$ by their leading-order values $C_i = f_i(0,0,0,0,0)$, the maps simplify to:

$$x' = C_2 \cos\phi + C_1 \rho^\delta \cos\theta, \qquad \alpha' = -\mu \cos\phi + C_3 \rho^\delta \cos\theta, \tag{18}$$

$$y' = C_2 \sin\phi + C_1 \rho^\delta \sin\theta, \qquad \beta' = -\mu \sin\phi + C_3 \rho^\delta \sin\theta, \tag{19}$$

where $-\mu = C_4$, factors of h are absorbed into the definitions of the C's, and (θ, ρ, ϕ) are given by the initial values of (x, α, y, β) on the section $r = h$. The intersection of $\mathcal{W}^{\mathrm{u}}$ with the Poincaré section $r = h$ can be found by setting $\rho = 0$: this results in $(\alpha', \beta') = -\mu(\cos\phi, \sin\phi)$, a circle with radius $|\mu|$, so clearly the global bifurcation occurs when μ crosses through zero.

Close enough to the global bifurcation, the ρ^δ terms will be small compared to C_2 so, dropping these terms from the (x', y') equations, there is a single equation for the angle θ':

$$\theta' = \begin{cases} \phi & \text{if } C_2 > 0, \\ \phi + \pi & \text{if } C_2 < 0, \end{cases} \tag{20}$$

and the map for (α, β) is:

$$\alpha' = -\mu \cos\phi + C \rho^\delta \cos\theta, \qquad \beta' = -\mu \sin\phi + C \rho^\delta \sin\theta, \tag{21}$$

where $C = C_3$.

The map (20–21) is the $O(2)$-symmetric version of the map describing the standard gluing bifurcation (see [21]): subspaces with $\theta = \phi \bmod \pi$ are invariant and can be seen to be attracting at least when $|\mu|$ is small and $\delta > 1$. Restricting to the invariant subspace $v = 0$ implies $y = \beta = 0$, $\cos\theta = \mathrm{sgn}(x)$ and $\cos\phi = \mathrm{sgn}(\alpha)$, where $\mathrm{sgn}(x)$ is 1 if $x > 0$ and -1 if $x < 0$. In this subspace, the gluing map is:

$$\cos\theta' = \mathrm{sgn}(C_2 \alpha), \qquad \alpha' = -\mu\, \mathrm{sgn}(\alpha) + C |\alpha|^\delta \cos\theta. \tag{22}$$

In the normal form (1–2), the value of the eigenvalue ratio δ at the gluing bifurcations is $1 + 1.6\sqrt{-\lambda}$ close to the Takens–Bogdanov point, with $P = -1$ and $Q = 2$, so $\delta > 1$ for all parameters of interest. When $\delta > 1$, the fixed points of the map (22) are approximately $\alpha = \pm\mu$ for $|\mu| \ll 1$ and $\mu < 0$. As μ increases through zero, these fixed points are replaced at the gluing bifurcation by period-two points $\alpha = \mu$, $\alpha = -\mu$.

Moving away from $L^2 = 0$ breaks the $O(2)$ symmetry of the map (20–21). The parameters μ and C will become functions of the angles θ and ϕ (as well as L^2) and the θ' map (20) will also be modified:

$$\theta' = \phi + \pi + D(\phi, \theta, L^2), \tag{23}$$
$$\alpha' = -\mu(\phi, \theta, L^2)\cos\phi + C(\phi, \theta, L^2)\rho^\delta \cos\theta, \tag{24}$$
$$\beta' = -\mu(\frac{\pi}{2} - \phi, \frac{\pi}{2} - \theta, L^2)\sin\phi + C(\frac{\pi}{2} - \phi, \frac{\pi}{2} - \theta, L^2)\rho^\delta \sin\theta, \tag{25}$$

where C_2 has been taken to be negative. The reflections that generate D_4 act on the variables $(\theta, \alpha, \beta, \phi)$ as

$$\mathcal{R}_1 : (\theta, \alpha, \beta, \phi) \to (\pi - \theta, -\alpha, \beta, \pi - \phi), \tag{26}$$
$$\mathcal{R}_2 : (\theta, \alpha, \beta, \phi) \to (\frac{\pi}{2} - \theta, \beta, \alpha, \frac{\pi}{2} - \phi), \tag{27}$$

so the functions $\mu(\phi, \theta)$, $C(\phi, \theta)$ and $D(\phi, \theta)$ must take the form

$$\mu = \mu_{00} + \mu_{20}\cos 2\phi + \mu_{11}\cos(\phi + \theta) + \mu_{02}\cos 2\theta + \mu_{40}\cos 4\phi + \ldots \tag{28}$$
$$C = C_{00} + C_{20}\cos 2\phi + C_{11}\cos(\phi + \theta) + C_{02}\cos 2\theta + C_{40}\cos 4\phi + \ldots \tag{29}$$
$$D = D_{40}\sin 4\phi + D_{31}\sin(3\phi + \theta) + \ldots \tag{30}$$

where all coefficients in the expressions above are of order L^2 apart from μ_{00} and C_{00}. The map (23–25) is the general form of the three-dimensional map that describes the dynamics near the gluing bifurcations in the normal form of the D_4-symmetric Takens–Bogdanov bifurcation, near the $O(2)$ limit. It contains many unknown parameters, and is quite unmanageable as it stands, but it can be reduced to a one-dimensional map by making further simplifications.

The two angles θ and ϕ refer respectively to the coordinates in the stable (x, y) and unstable (α, β) directions at the origin. Close to the gluing bifurcation, trajectories arrive at the origin with $\rho \approx \mu$, with $\rho < h \ll 1$. It follows from the map near the origin (13), and from the fact that $\delta > 1$, that trajectories leave the neighbourhood of the origin with $r < h$, while the exit value of ρ is $\rho = h$. By making the additional restriction that $\mu \ll h$ (i.e., close enough to the gluing bifurcation), it follows that the exit value of r satisfies $r \ll h$, so the values of the stable coordinates (α, β) are very much larger than the values of the stable coordinates (x, y) on leaving the origin. The fate of global part of the trajectory will then depend mainly on $(\alpha, \beta) = h(\cos\phi, \sin\phi)$, and so at leading order the three parameters μ, C and D will be functions of ϕ (and L^2) only, and not of θ. This surprising result is confirmed numerically in section 4.

In addition, with $\delta > 1$, the ρ^δ terms in the map will be small compared to μ, close enough to the gluing bifurcation, and so can be dropped. Effectively this assumes that all trajectories leave on $\mathcal{W}^{\mathrm{u}}$; the assumption is equivalent to that made when writing $\alpha = -\mu$ as the fixed point of the map (22).

With these two simplifications (which can be justified when $L^2 \ll 1$ and $\mu \ll h \ll 1$), the map (23–25) reduces to

$$\alpha' = -(\mu + A\cos 2\phi + B\cos 4\phi + \ldots)\cos\phi, \tag{31}$$

$$\beta' = -(\mu - A\cos 2\phi + B\cos 4\phi + \ldots)\sin\phi, \tag{32}$$

where $\mu = \mu_{00}$, $A = \mu_{20}$ and $B = \mu_{40}$. This map is actually a one-dimensional circle map, as (α', β'), which lies on the circle $\rho' = h$, determines the value of ϕ' for the next iterate:

$$\phi' = \tan^{-1}\left(\frac{\mu - A\cos 2\phi + B\cos 4\phi}{\mu + A\cos 2\phi + B\cos 4\phi}\tan\phi\right) \equiv g(\phi), \tag{33}$$

where the branch of $\tan^{-1}$ is chosen so that ϕ' is in the correct quadrant, as specified by the signs of α' and β'. The Fourier series for $\mu(\phi)$ has been truncated to the first three terms, which is sufficient to include the range of possible behaviour observed in the ODEs below.

4 Bifurcations in the map and normal form

The map $g(\phi)$, illustrated in figure 3, has D_4 symmetry, where the two reflections act on ϕ as specified in (26–27). The gluing bifurcation occurs in the $v = 0$ subspace when $\mu = -B - A$ and in the $u = v$ subspace when $\mu = B$. With the illustrative choice of parameters $A = -1.8$ and $B = 1.2$ (guided by numerical results presented below), the gluing bifurcation occurs in the $v = 0$ subspace first as μ is increased. These two subspaces are forward-invariant but, within the context of the one-dimensional map, the subspaces have lost the reverse-invariance that would normally be inherited from the ODEs.

It is readily apparent that the values $\phi = 0$ (in the $v = 0$ subspace) and $\phi = \frac{1}{4}\pi$ (in the $u = v$ subspace) etc. are either fixed points or period-two points of the map (33). The slope of the map at 0 and $\frac{1}{4}\pi$ is

$$g'(0) = \frac{\mu + B - A}{\mu + B + A}, \qquad g'(\tfrac{1}{4}\pi) = \frac{-\mu + B - 2A}{-\mu + B}, \tag{34}$$

so there are symmetry-breaking bifurcations from the $\phi = 0$ fixed point, when it loses stability at $\mu = -B$, and from the $\phi = \frac{1}{4}\pi$ period-two point, when it gains stability at $\mu = B - A$. Thus within the invariant subspaces, there are gluing bifurcations as usual, but there is a range of parameters $-B < \mu < B - A$ in which neither subspace is stable.

The mechanism by which stability is transfered from one subspace to the other is summarised in figure 4. This bifurcation diagram corresponds to the same cut through parameter space as in figure 1(c). The details are quite involved because of the period-doubling cascades, chaotic trajectories and periodic windows expected in multi-modal maps of this type, and could be analysed using techniques described in [22]. There are parameter intervals with chaotic trajectories of five different symmetry types. The transfer of stability is illustrated using a sequence of parameters in figure 5. These show intersections of chaotic

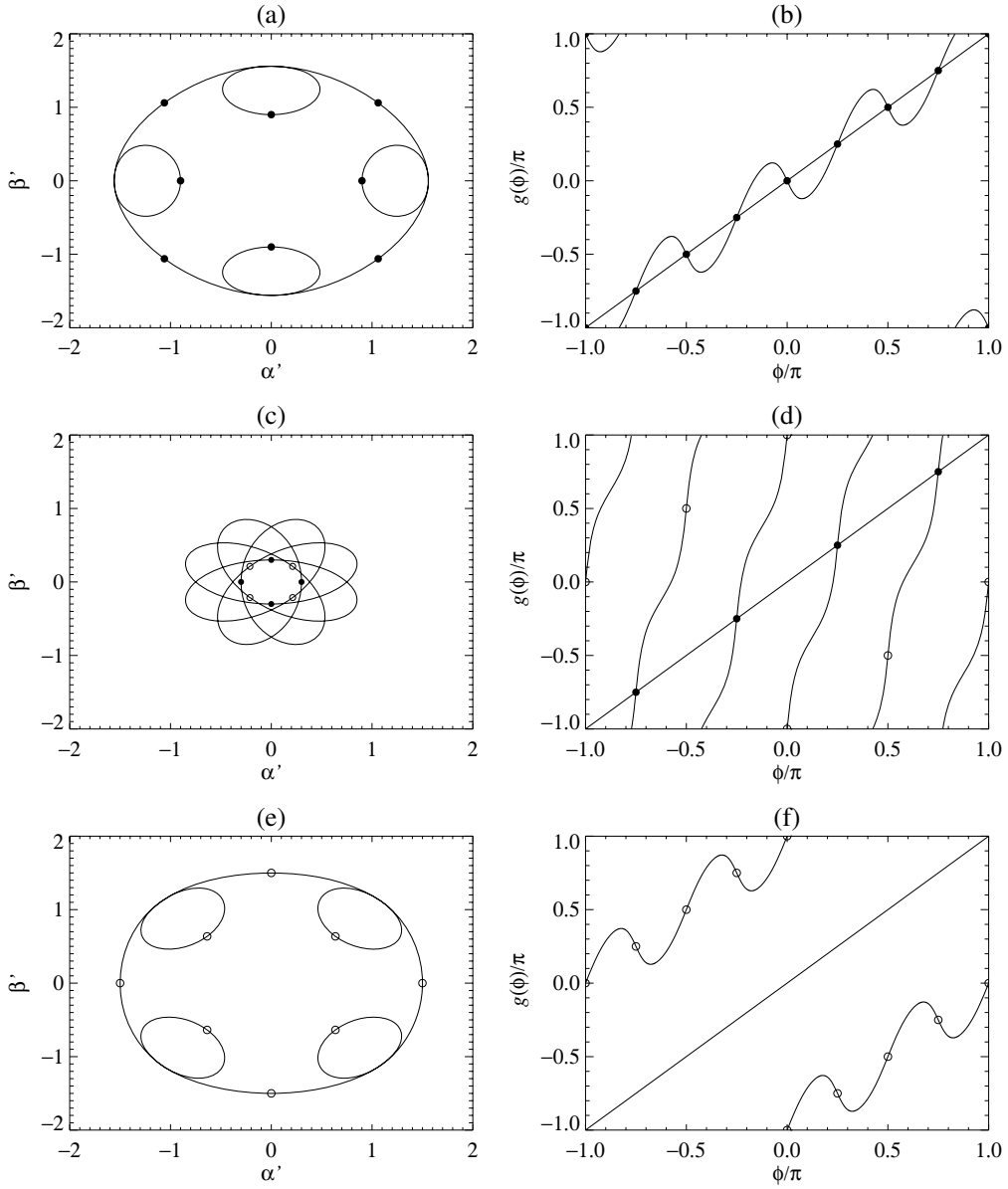

Fig. 3. The one-dimensional map: (a,c,e): (α', β') as a function of ϕ, from (31–32); (b,d,f): $g(\phi)$, from (33). Illustrative values are chosen: $A = -1.8$, $B = 1.2$, and (a,b): $\mu = -0.3$ (before both gluing bifurcations); (c,d): $\mu = 0.9$ (between the two gluing bifurcations); (e,f): $\mu = 2.1$ (after both gluing bifurcations). Fixed points of the map are indicated by filled circles and period-two points by open circles. The lines in the (α', β') plane in (a,c,e) represent the intersection of the unstable manifold of the origin $\mathcal{W}^{\mathrm{u}}$ with the Poincaré plane $r = h$.

trajectories of the ODEs (1–2) with the Poincaré plane $r = h = 2 \times 10^{-5}$, as well as the one-dimensional map (33) with parameters (given in table 1) determined from the ODE data by least-squares fitting. The ODEs were integrated using the Bulirsch–Stoer method [23] with a relative local truncation error of 10^{-12}, sufficient to provide accurate solutions in spite of the very small

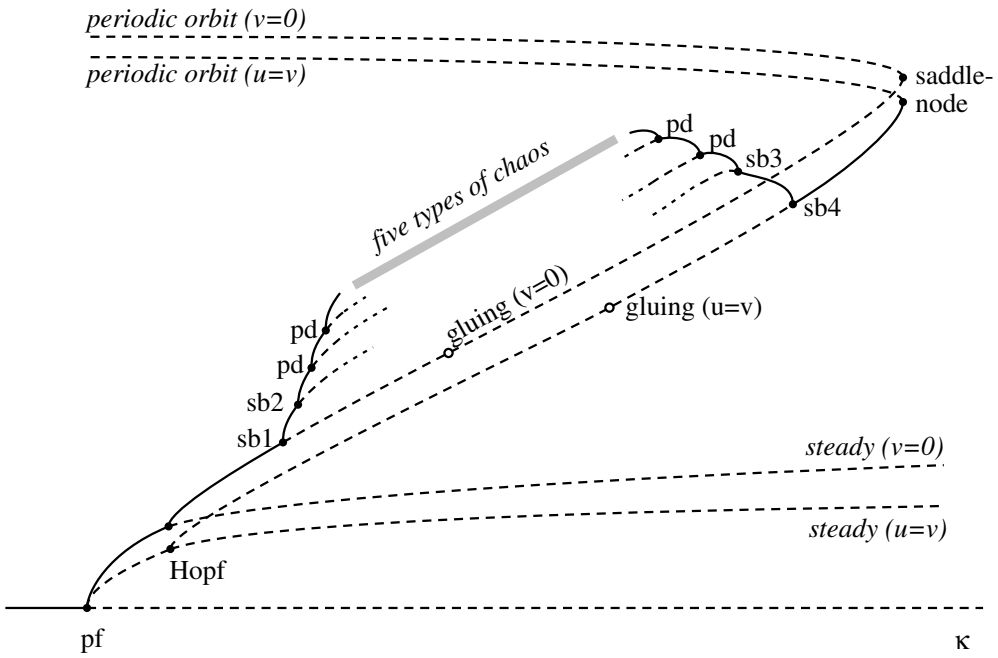

Fig. 4. Bifurcation diagram of the Takens–Bogdanov normal form (1–2) near the $O(2)$ limit – see figure 1(c). The initial pitchfork bifurcation yields stable equilibria in the $v = 0$ subspace and unstable equilibria in the $u = v$ subspace. These undergo Hopf bifurcations and the resulting periodic orbits undergo gluing bifurcations within the subspaces. Stability is transfered from one to the other via symmetry-breaking (sb) bifurcations, period-doubling (pd) bifurcations and an interval of chaotic dynamics involving chaotic attractors with five different symmetry types. The picture of the dynamics between the leftmost and rightmost symmetry-breaking bifurcations is derived from the one-dimensional map (33).

differences in the parameter values.

We have not included in figure 4 any details about other periodic orbits that are created in the primary Hopf bifurcation with D_4 symmetry, such as rotating waves [24]. Any such orbits will not participate in the dynamics close to the global bifurcations of interest here.

With μ very negative, the fixed point $\phi = 0$ in the $v = 0$ subspace is stable, and it loses stability in a supercritical symmetry-breaking bifurcation (sb1 in figure 4) as the Floquet multiplier passes through -1. The spatio-temporal symmetry of the new orbit is lost in another symmetry-breaking bifurcation (sb2), which is followed by a period-doubling cascade, ending up as in figure 5(a,b) with chaotic trajectories that have no symmetry even when considered as a set. Set-wise reflection symmetry is gained when this chaotic attractor crosses the $v = 0$ subspace (figure 5c,d), and the full D_4 symmetry is achieved when this new chaotic set in turn crosses the $u = v$ subspace (figure 5e,f). The D_4 symmetry is retained as μ is increased through the two gluing bifurcations within the invariant subspaces (compare figure 5g,h and 3c,d). D_4 symmetry is then lost as the chaotic trajectory ceases to intersect the $v = 0$ subspace

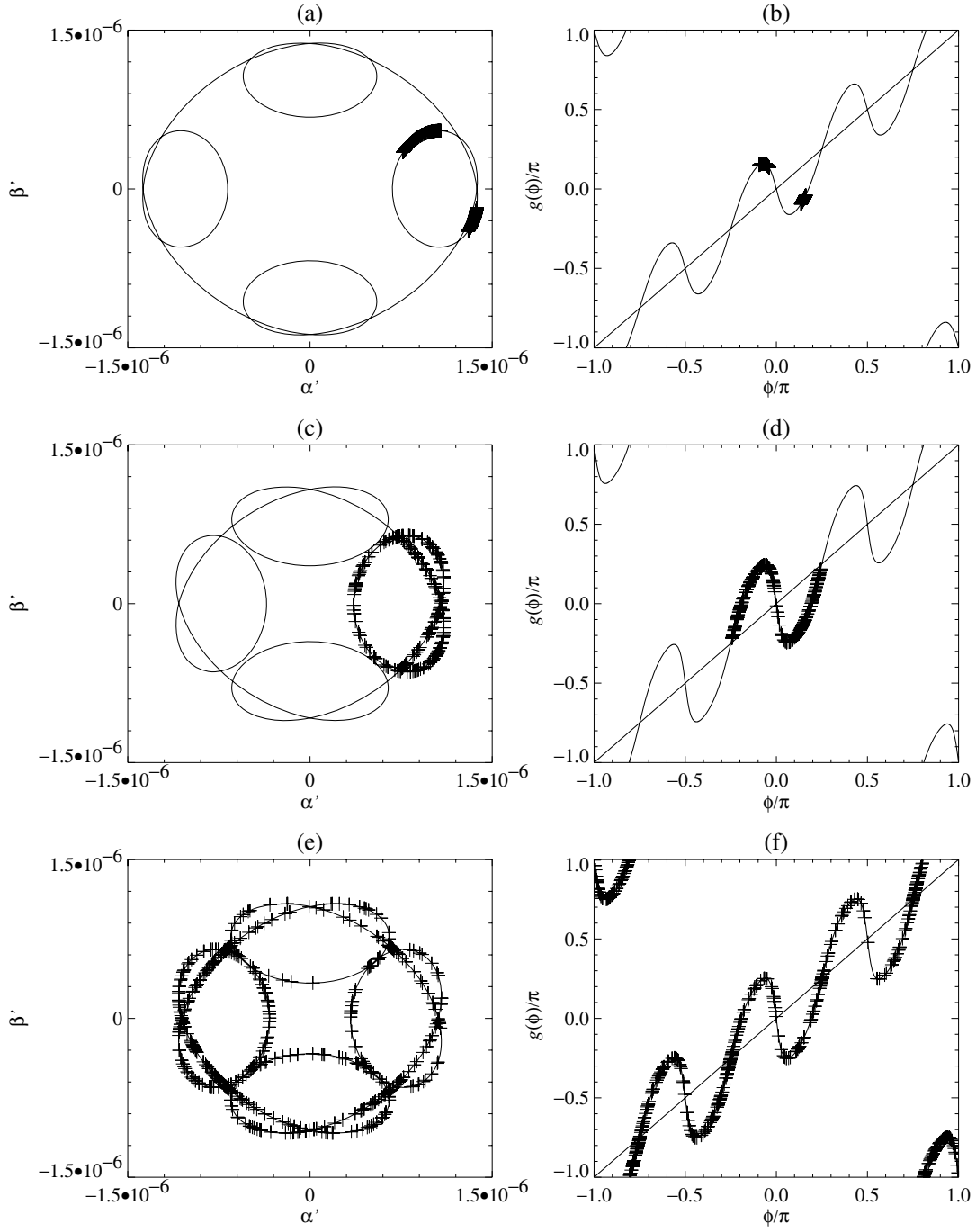

Fig. 5. Comparing the one-dimensional map to the dynamics of the normal form (1–2), with $L^2 = 10^{-8}$, $\lambda = -0.1$ and: (a,b): $\kappa = -0.1611146069$; (c,d): $\kappa = -0.1611146056$; (e,f): $\kappa = -0.1611146055$. The + symbols in the left panels represent intersections of a single chaotic trajectory with the Poincaré plane $h = 2 \times 10^{-5}$, while in the right panels, successive values of ϕ for the ODE trajectory are plotted against each other. The solid lines are a least-squares fit of (33) to the ODE data, with fitted parameters given in table 1. The lines have the same significance as in figure 3.

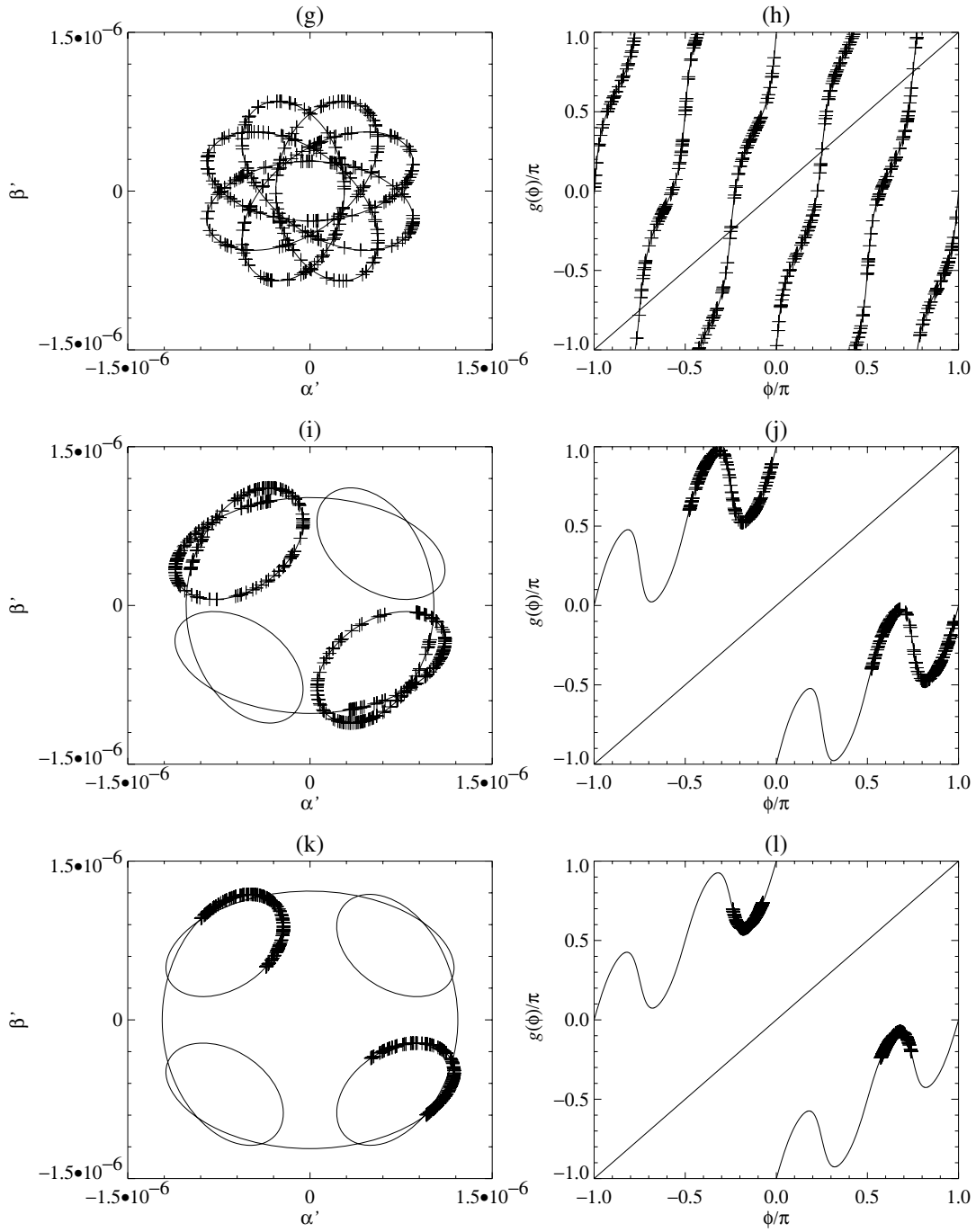

Fig. 6. continued from figure 5. (g,h): $\kappa = -0.1611146030$; (i,j): $\kappa = -0.1611146000$; (k,l): $\kappa = -0.1611145992$.

(figure 5i,j) and then reflection symmetry is lost in figure 5(k,l). An inverse period-doubling cascade, followed by two inverse symmetry-breaking bifurcations (sb3 and sb4), leads to the period-two orbit in the $u = v$ subspace gaining stability. This sequence, along with the other bifurcations known from the ODEs, is summarised in figure 4.

Figure 5	κ	$\mu/(L^2\|\lambda\|)$	$A/(L^2/\lambda\|)$	$B/(L^2\|\lambda\|)$
(a,b)	-0.1611146069	-77.6	-1812.660	1212.380
(c,d)	-0.1611146056	242.2	-1812.667	1212.311
(e,f)	-0.1611146055	266.8	-1812.668	1212.359
(g,h)	-0.1611146030	882.0	-1812.664	1212.351
(i,j)	-0.1611146000	1620.2	-1812.670	1212.355
(k,l)	-0.1611145992	1817.1	-1812.676	1212.261

Table 1
Parameters in the one-dimensional map (33) determined from the ODE data in figure 5 by least-squares fitting. The parameters scale with L^2 and $|\lambda|$ and depend on the choice of Poincaré plane h. The ODE data is fitted to within one part in 10^4, which is consistent with the simplifications made in deriving the map. Note that μ increases linearly with κ while A and B are nearly independent of κ. The excellent fit of the one-dimensional map to the ODE data confirms that μ, C and D in (28–30) do not depend on θ at leading order.

As an interesting aside, note that the sequence of symmetry groups displayed by the chaotic sets as a whole in figure 5(a,c,g,i,k) is: no symmetry, Z_2, D_4, D_2 and Z_2. Changes of symmetry occur when the chaotic attractor collides with an invariant subspace [25]. However, in figure 5(a,i,k), the chaotic set is made up of two disjoint parts: trajectories alternate between them, so for the second iterate of the map, the symmetry types of the chaotic sets would be: no symmetry, Z_2, D_4, Z_2 and no symmetry. The last two of these have chaotic versions of spatio-temporal symmetries. The map has periodic orbits with Z_4 symmetry, but no examples of chaotic sets with this symmetry have been found, consistent with the analysis of [26].

The entire sequence of bifurcations described here depends (in the one-dimensional map) only on the relative positions of the parameters A and B (one of which can be scaled to be equal to 1). There are other possible orders of the bifurcations, but overall these will be broadly similar to the one already described, at least in the cases where one or other of the two invariant subspaces is stable for μ large enough.

In the Z_2- and $O(2)$-symmetric problems, the unfolding diagram of the Takens–Bogdanov bifurcation has a single line of gluing bifurcations (as in figure 1a). In the D_4 case near the $O(2)$ integrable limit, this single line splits into two lines whose slopes differ by an amount of order L^2. At a fixed small value of λ, the map bifurcation parameter μ depends linearly on κ. Three pieces of information are required to establish the values of A and B along with the relation between μ and κ. Two of these are provided by the known locations of the gluing bifurcations (6), along with the relation between μ, A and B at the two gluing bifurcations in the map. The third could be provided by, for instance, the location of the symmetry-breaking bifurcation at which the periodic orbit

in the $v = 0$ subspace loses stability to transverse perturbations; determining this would require evaluations of elliptic integrals and is in principle do-able by hand [12], or the bifurcation could be located numerically. With this third piece of information, the scale is set, and the locations of all the other bifurcations found in the map can be predicted for the ODEs. In particular, the wedge of parameters between the two gluing bifurcations, extending right to the Takens–Bogdanov codimension-two point, contains chaotic trajectories that are set-wise D_4 symmetric.

5 Discussion

The main conclusion of this work is that the dynamics of the normal form of the Takens–Bogdanov bifurcation with D_4 symmetry appears to be governed by a one-dimensional map near the gluing bifurcation and near the $O(2)$ integrable limit, rather than the three-dimensional map one would expect. This is a great simplification, and it allows a quantitative description of the bifurcation sequence through which stability is transfered from one subspace ($v = 0$) to the other ($u = v$), through a sequence of symmetry-breaking and period-doubling bifurcations and chaotic sets with five different symmetry types. The arguments made in deriving the one-dimensional map apply in general, not just to the specific model of magnetoconvection considered here. This work provides at least a starting point for understanding the complications inherent in the D_4-symmetric Takens–Bogdanov bifurcation.

The arguments made in this paper for reducing the map from three to one dimension are persuasive rather than rigorous. More work is needed to put the simplifications outlined here on a firmer footing. Further from the $O(2)$ limit, when the gluing bifurcations in the invariant subspaces are not quite so close together, the order L^2 corrections cannot be neglected and there will be a transition from one-dimensional to three-dimensional dynamics.

This work is complementary to the approach taken for the D_3-symmetric Takens–Bogdanov bifurcation by Matthies [9], who did not assume proximity to the $O(2)$ limit (the approach could readily be modified for the D_4 case). Matthies was able to prove the existence of a subshift of finite type, for those trajectories that repeatedly visit the neighbourhood of the origin; however, such trajectories are not stable, and almost all trajectories eventually stop returning to a neighbourhood of the origin. The advantage of taking the $O(2)$ limit is that near the gluing bifurcations, all trajectories leaving a neighbourhood of the origin will return there, so the dynamics described here can be observed in ODEs and physical systems.

Acknowledgements

I have benefited from interesting conversations with Peter Ashwin, Jon Dawes, Paul Glendinning, Edgar Knobloch, Paul Matthews and Marty Golubitsky, and I am grateful for support from the Engineering and Physical Science Research Council.

References

[1] S. Chandrasekhar, *Hydrodynamic and Hydromagnetic Stability* (Clarendon Press, Oxford, 1961).

[2] E. Knobloch and M.R.E. Proctor, Nonlinear periodic convection in double-diffusive systems, *J. Fluid Mech.* **108** (1981) 291–316.

[3] A.M. Rucklidge, Chaos in models of double convection, *J. Fluid Mech.* **237** (1992) 209–229.

[4] M.R.E. Proctor and N.O. Weiss, Magnetoconvection, *Rep. Prog. Phys.* **45** (1982) 1317–1379.

[5] P.H. Coullet and E.A. Spiegel, Amplitude equations for systems with competing instabilities, *SIAM J. Appl. Math.* **43** (1983) 776–821.

[6] J. Guckenheimer and E. Knobloch, Nonlinear convection in a rotating layer: amplitude expansions and normal forms, *Geophys. Astrophys. Fluid Dynamics* **23** (1983) 247–272.

[7] D. Armbruster, J. Guckenheimer and S. Kim, Chaotic dynamics with square symmetry, *Phys. Lett. A* **140** (1989) 416–420.

[8] Y.Y. Renardy, M. Renardy and K. Fujimura, Takens–Bogdanov bifurcation on the hexagonal lattice for double layer convection, *Physica* **129D** (1999) 171–202.

[9] K. Matthies, A subshift of finite type in the Takens–Bogdanov bifurcation with D_3 symmetry, *Doc. Math. J. DMV* **4** (1999) 463–485.

[10] J. Guckenheimer and P. Holmes, *Nonlinear Oscillations, Dynamical Systems and Bifurcations of Vector Fields* (Springer, New York, 1983).

[11] A.K. Thomas, The Takens–Bogdanov bifurcation with D_4 symmetry, *preprint* (2000).

[12] G. Dangelmayr and E. Knobloch, The Takens–Bogdanov bifurcation with $O(2)$-symmetry, *Phil. Trans. R. Soc. Lond. A* **A322** (1987) 243–279.

[13] P. Hirschberg and E. Knobloch, Complex dynamics in the Hopf bifurcation with broken translation symmetry, *Physica* **90D** (1996) 56–78.

[14] A.S. Landsberg and E. Knobloch, Oscillatory bifurcation with broken translation symmetry, *Phys. Rev. E* **53** (1996) 3579–3600.

[15] J. Moehlis and E. Knobloch, Bursts in oscillatory systems with broken D_4 symmetry, *Physica* **135D** (2000) 263–304.

[16] S.A. Campbell and P. Holmes, Heteroclinic cycles and modulated traveling waves in a system with D_4 symmetry, *Physica* **59D** (1992) 52–78.

[17] A.M. Rucklidge, Symmetry-breaking instabilities of convection in squares, *Proc. R. Soc. Lond.* A **453** (1997) 107–118.

[18] G.B. Mindlin, T. Ondarçuhu, H.L. Mancini, C. Pérez-García and A. Garcimartín, Comparison of data from Bénard–Marangoni convection in a square container with a model based on symmetry arguments, *Int. J. Bifurcation and Chaos* **4** (1994) 1121–1133.

[19] M.R.E. Proctor and N.O. Weiss, Normal forms and chaos in thermosolutal convection, *Nonlinearity* **3** (1990) 619–637.

[20] A.M. Rucklidge, Chaos in magnetoconvection, *Nonlinearity* **7** (1994) 1565–1591.

[21] D.V. Lyubimov and S.L. Byelousova, Onset of homoclinic chaos due to degeneracy in the spectrum of the saddle, *Physica* **62D** (1993) 317–322.

[22] M. Krupa and M. Roberts, Symmetry breaking and symmetry locking in equivariant circle maps, *Physica* **57D** (1992) 417–435.

[23] W.H. Press, B.P. Flannery, S.A. Teukolsky and W.T. Vetterling, *Numerical Recipes – the Art of Scientific Computing* (Cambridge University Press, Cambridge, 1986).

[24] J.W. Swift, Hopf bifurcation with the symmetry of a square, *Nonlinearity* **1** (1988) 333–377.

[25] P. Chossat and M. Golubitsky, Symmetry-increasing bifurcation of chaotic attractors, *Physica* **32D** (1988) 423–436.

[26] I. Melbourne, M. Dellnitz and M. Golubitsky, The structure of symmetric attractors, *Arch. Rat. Mech. Anal.* **123** (1993) 75–98.